ORIGINAL PAPER

Dynamic characteristics and influencing factors of precipitation $\delta^{18}O$, China

Huiwen Guo[1] · Guofeng Zhu[1,2] · Yuanqing He[2] · Junju Zhou[1] · Hanxiong Pan[1] · Xianggang Ma[1] · Yu Zhang[1] ·
Meihua Huang[1] · Juan Xiang[1]

Abstract

It is the basis of isotope technology application to clarify which factors are related to precipitation isotopes in different regions. China has a vast territory, and there is still no comprehensive and systematic understanding of the spatial distribution pattern and influencing factors of precipitation stable isotopes in China. Based on the known Bowen and Wilkinson model, the latitude and altitude of 117 sites in China were used to simulate $\delta^{18}O$ value of each site and to generate the high precision spatial distribution map of the precipitation oxygen stable isotope over China. According to the spatial distribution of precipitation $\delta^{18}O$, the basic effects of isotope variation in different climatic regions were analyzed: latitude effect, elevation effect, temperature effect, precipitation effect, and water vapor source and transportation process. In the eastern monsoon region, the latitude effect of isotope variation is shown, but the difference between the southern region and the northern region is large. The southern region is affected by the water vapor of the subtropical Pacific Ocean and precipitation amount effect to form a high value area of $\delta^{18}O$, and the northern region is more susceptible to the temperature effect. In the same latitude area, due to the influence of local recycled water vapor and local evaporation, a high-value area of $\delta^{18}O$ is formed in the inland basin of the northwestern arid region. In the Qinghai–Tibet Plateau, the isotope values affected by the high terrain are generally low. The change of $\delta^{18}O$ value reflects the extent to which the south and north areas of the Qinghai–Tibet Plateau are affected by the southwest monsoon and local water vapor.

1 Introduction

Stable isotopes (^2H, ^{18}O) are components of natural water body and are very sensitive to environmental changes (Dansgaard 1953; Craig 1961). They record the internal information of water cycle process and are an effective method to track complex hydrological and climatic processes (Gat 1996; Clark and Fritz 1997; Edwards et al. 2010; Good et al. 2015). The stable isotope composition of precipitation not only provides a means for the study of modern processes of global and regional climate and hydrology but also is applied to quantitative paleoclimate reconstruction (Hoffmann and Heimann

1997; Johnson and Ingram 2004; Daley et al. 2012; Fernandoy et al. 2011). All of these studies require more information on stable isotopes in precipitation.

At present, the global network for isotope in precipitation (GNIP) has more than 1000 monitoring sites, but only 31 stations are included in China, and the development of large-scale isotope monitoring network is relatively slow. Based on the experience of GNIP and other countries in establishing isotope observation networks, China has successively established a series of precipitation isotope monitoring networks, such as the Chinese Network of Isotopes in Precipitation (CHNIP) (Song et al. 2007) and the Tibetan Plateau Network of Isotopes in Precipitation (TNIP) (Yao et al. 2013). Scholars have applied the precipitation isotope data of these sites to carry out a lot of basic research and applied research, which has promoted the development of isotope theory. In the 1950s, Dansgaard (1953) discovered that isotopes in precipitation gradually depleted as the condensation temperature decreased, which opened up the application of isotopes in the field of hydrological cycles. Subsequently, many scholars began to explore the factors affecting the variation of precipitation isotope values (Craig

✉ Guofeng Zhu
  gfzhu@lzb.ac.cn; guofengzhu@me.com

[1] College of Geography and Environment Science, Northwest Normal University, 967 Anning Eest Road, Lanzhou 730070, Gansu, China

[2] State Key Laboratory of Cryosphere Sciences, Northwest Institute of Eco-Environment and Resources, Chinese Academy of Sciences, Lanzhou 730000, Gansu, China

1961; Gat 1980; Liu et al. 2009a, b; Zhu et al. 2016). The atmospheric circulation model was used to study the variation characteristics of large-scale precipitation stable isotopes (Tindall et al. 2009; Sjolte et al. 2011; Zhang et al. 2012; Samuels-Crow et al. 2014). The relationship between precipitation isotopes and climatic factors was discussed and the sources of precipitation water vapor was analyzed (Pang et al. 2005; Sengupta and Sarkar 2006; Yamanaka et al. 2007; Li et al. 2014). In addition, a large number of studies have been carried out in the Qinghai–Tibet Plateau (Tian et al. 2001; Yao et al. 2013), the southwest monsoon region (He et al. 2000; Pu et al. 2013), the southeast monsoon region and the northwest arid region (Liu et al. 2008, 2009a; Huang et al. 2015; Wang et al. 2018), as well as on the basin scale (Wu et al. 2011; Zhao et al. 2011; Li et al. 2013a; Pang et al. 2015; Zhu et al. 2019) in China.

The research of precipitation isotopes in China has been fruitful on the regional scale, but for a long time, it has been difficult to observe in some areas (high latitude and high altitude) on the national scale and the data sharing of existing observation stations is insufficient. Therefore, it is necessary to establish the spatial distribution pattern of precipitation isotopes in China according to the modeling methods of Bowen and Wilkinson (2002, hereinafter referred to as BW model) to make up for the precipitation isotopes blanks of the lacks observation areas. The BW model has been used in previous research and is worthy of reference (Bowen and Wilkinson 2002; Dutton et al. 2005; Liu et al. 2009b), but further studies expanding the available data and exploring the implications of precipitation isotope variability in China are needed. In this study, the annual mean $\delta^{18}O$ data of 177 sites (including 99 observation sites and 8 ice core sampling sites) was used to (1) re-establish the spatial distribution pattern of precipitation isotopes across China and (2) invert the atmospheric hydrological process and analyze the influencing factors of precipitation isotope changes in different climate regions of China. This study improves the accuracy of spatial distribution of precipitation isotopes over China and provides a new platform for understanding the spatial variability and influencing factors of precipitation stable isotope in China.

2 Data and method

2.1 Data sources

A total of 117 $\delta^{18}O$ data including precipitation observation sites and ice core sampling points were collected. Figure 1 shows the spatial distribution of these sites in China. Among them, the $\delta^{18}O$ data of 31 sites is from the GNIP dataset (http://www-naweb.iaea.org), our research team provides the measured $\delta^{18}O$ data of 3 sites, and the remaining 83 sites are from publicly published research results in domestic and international journals. Detailed data information for each site is listed in Table 1. The precipitation isotope data provided by

GNIP, the technical procedures for sample collection and transportation, and the standard data are strictly formulated by the International Atomic Energy Agency (IAEA). The isotope analysis was performed by the laboratory of the institute of cooperation of member states through sample comparison, and all analytical errors were controlled. In addition to GNIP sites, Chinese scholars and research institutions have established precipitation sample collection sites nationwide to measure isotope data by referring to GNIP sampling and experimental procedures. The error of the precipitation samples of each site is the measurement error of the analyzer itself. When selecting these sites, the measurement error of the precipitation $\delta^{18}O$ value is controlled to be between ± 0.1 and $\pm 0.5‰$. All of the above measured oxygen isotope data is expressed as δ values relative to V-SMOW (Vienna Standard Mean Ocean Water):

$$\delta^{18}O = \frac{R_{\text{sample}} - R_{\text{standard}}}{R_{\text{standard}}} \times 1000‰, \tag{1}$$

where R_{sample} is the ratio of $^{18}O/^{16}O$ in the samples and R_{standard} is the ratio of $^{18}O/^{16}O$ in V-SMOW.

The $\delta^{18}O$ value of precipitation is the weighted mean of precipitation amount for one or more years, calculated as follows:

$$\delta_{(w)} = \sum P_i \delta_i / \sum P_i, \tag{2}$$

where P_i is the precipitation amount and δ_i is the oxygen isotope value .

In addition, the long-term climatic data were derived from the WorldClim-Global Climate Data version 2 (http://www.world-clim.org) (Fick and Hijmans 2017) and are also listed in Table 1. The vapor flux was calculated using NCEP/NCAR $2.5° \times 2.5°$ reanalysis data (NCEP/NCAR Reanalysis 1), which were obtained from the National Center for Environmental Prediction/National Center for Atmospheric Research (http://www.esrl.noaa.gov).

2.2 BW model

Bowen and Wilkinson (2002) established a spatial distribution model of precipitation oxygen isotope (referred to as the BW model), which is one of the most effective methods for estimating the spatial distribution of stable isotopes in precipitation (Bowen and Revenaugh 2003). The BW model considers that the isotopic composition of precipitation as the sum of temperature driven rainout effect and regional patterns of water vapor source and transport (Bowen and Revenaugh 2003). Usually, the temperature is mainly affected by latitude and altitude, so the BW model uses altitude and latitude as model parameters to simulate the $\delta^{18}O$ value (Liu et al. 2009b). The BW model is expressed as follows:

$$\delta^{18}O = a|\text{Lat}|^2 + b|\text{Lat}| + c\text{Alt} + d, \tag{3}$$
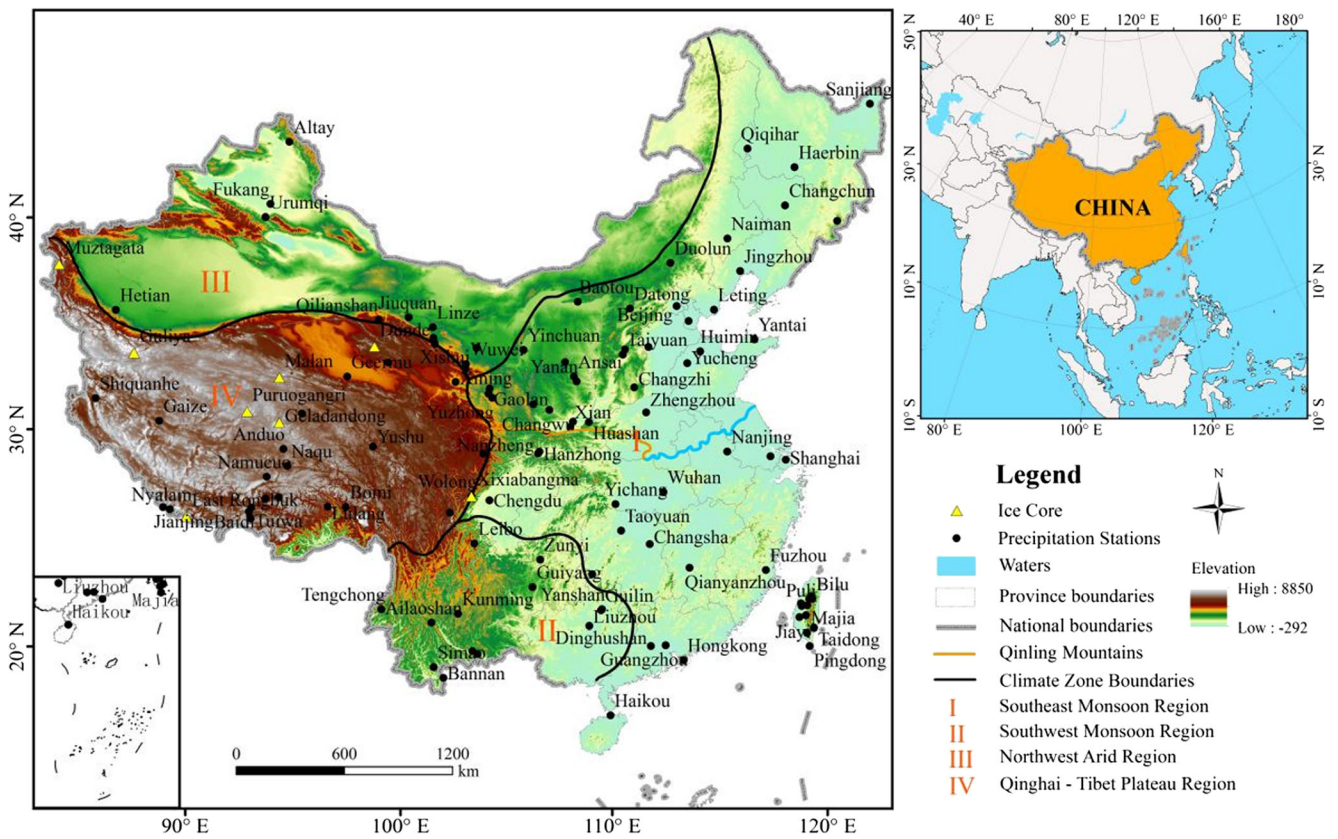
Fig. 1 Spatial distribution of precipitation observation sites and ice core sampling sites and different climatic zones (the southeastern monsoon region can be divided into the southern region and the northern region with the boundary of the Qinling-Huaihe River) in China

where δ^{18}O is the preliminary estimated annual mean precipitation oxygen isotope value. Lat and Alt is the latitude (°) and altitude (m) of observation site, respectively. a, b, and c are empirical parameters; d is an intercept. The error of the BW model was assessed using mean bias error (MBE), mean absolute error (MAE), and root mean square error (RMSE). According to the BW model (Bowen and Wilkinson 2002; Bowen and Revenaugh 2003), the final spatial distribution pattern of precipitation isotope is a combination of model estimates and interpolated residual error using inverse distance weighted method in Arcgis 10.2 software.

3 Results and discussion

3.1 Basic pattern

It can be seen from the method that the BW model is a second-order polynomial regression model of δ^{18}O and latitude and altitude. During the process of water vapor transport from low latitude to high latitude, water vapor condensation produces precipitation due to the gradual decrease of temperature, which makes the residual water vapor and the isotopes in the subsequent precipitation gradually depleted, showing the latitude effect of the change of isotope value. In addition to the

latitude effect, with the increase of altitude, the isotope value also shows a decreasing trend, that is, the elevation effect of the change of isotope value. In order to make the model effect more ideal, the BW model adopts a two-step regression method, which avoids the interaction of latitude effect and elevation effect. In order to minimize the effects of height, based on previous research experience (Bowen and Wilkinson 2002; Dutton et al. 2005) and the distribution of Chinese sites (Fig. 1), the first fit is the latitude and δ^{18}O values of the site elevation below 200 m ($n = 31$). A second-order polynomial best describes the dependence of δ^{18}O value on latitude:

$$\delta^{18}O = -0.009\text{Lat}^2 + 0.427\text{Lat} - 11.323 \qquad (4)$$
$$\left(r^2 = 0.92, P < 0.0001\right),$$

It can be seen from Eq. (4) that the goodness of fit between δ^{18}O and latitude is high, and there is a significant negative correlation between them. Figure 2a also shows that as the latitude increases, the δ^{18}O value decreases gradually. Therefore, the isotope values of sites below 200 m over China show better latitude effect. The latitude effect is more obvious to the north of 30 °N (Fig. 2a).

The large elevation difference of China's topography is an advantageous condition for studying the isotope elevation effect. In this study, the altitude of all sites ranged from 3 to

Table 1 Basic information of precipitation observation sites and ice core sampling sites and their $\delta^{18}O$ value in China

Sites	Long (°E)	Lat (°N)	Alt (m)	Annual mean			Data sources
				T (°C)	P (mm)	$\delta^{18}O$ (‰)	
Tianjin	117.10	39.06	3	12.95	540	− 7.68	GNIP
Guangzhou	113.32	23.13	7	22.09	1692	− 5.83	GNIP
Haikou	110.21	20.02	15	24.40	1711	− 6.09	GNIP
fuzhou	119.17	26.05	16	19.93	1361	− 6.6	GNIP
Wuhan	114.13	30.62	23	17.00	1236	− 6.67	GNIP
Nanjing	118.18	32.18	26	15.44	979	− 7.26	GNIP
Changsha	113.04	28.12	37	17.66	1424	− 6.69	GNIP
Hong Kong	114.17	22.32	66	22.40	2166	− 6.64	GNIP
Jinzhou	121.10	41.13	66	9.10	560	− 8.54	GNIP
Yantai	121.10	37.53	66	11.98	651	− 7.24	GNIP
Shijiazhuang	114.25	38.02	80	12.71	505	− 8.05	GNIP
Liuzhou	109.40	24.35	97	20.86	1614	− 6.47	GNIP
Zhengzhou	113.65	34.72	110	14.65	627	− 7.04	GNIP
Qiqihar	123.55	47.23	147	3.62	414	− 10.6	GNIP
Yanshan	110.08	25.07	170	19.19	1885	− 5.96	GNIP
Haerbin	126.62	45.68	172	4.32	542	− 10.2	GNIP
Changchun	125.22	43.9	237	5.18	591	− 10.09	GNIP
Xi'an	108.93	34.3	397	14.07	624	− 7.41	GNIP
Chengdu	104.02	30.67	506	16.57	928	− 7.05	GNIP
Taiyuan	112.55	37.78	778	10.25	422	− 8.89	GNIP
Zunyi	106.88	27.7	844	15.41	1068	− 8.32	GNIP
Urumqi	87.62	43.78	918	7.23	231	− 10.7	GNIP
Guiyang	106.43	26.35	1071	14.91	1147	− 8.33	GNIP
Yinchuan	106.13	38.29	1112	9.13	198	− 6.62	GNIP
Jinbian	108.79	37.61	1337	8.28	398	− 7.6	GNIP
Hetian	79.56	37.08	1375	11.67	30	− 5.74	GNIP
Lanzhou	103.88	36.05	1517	8.93	345	− 5.47	GNIP
Pingliang	106.68	35.51	1800	8.82	524	− 9.3	GNIP
Kunming	102.41	25.01	1892	14.87	886	− 10.26	GNIP
Shanghai	121.48	31.22	4	16.46	1061	− 7.47	Yang et al. (2014)
Leting	118.88	39.43	10.5	10.81	620	− 8.26	Pang et al. (2015)
Huimin	117.53	37.43	11.7	13.26	583	− 7.99	Pang et al. (2015)
Yucheng	116.60	36.95	20	13.52	590	− 8.2	Yang et al. (2014)
Jiayi	120.46	23.48	27	23.20	1901	− 6.02	Peng et al. (2010)
Taizhong	120.68	24.12	34	22.38	1807	− 6.03	Peng et al. (2010)
Beijing	116.46	39.92	43	12.40	557	− 8.77	Yang et al. (2014)
Pingdong	120.80	22.03	54	23.83	2465	− 6.41	Peng et al. (2010)
Sanjing	133.52	47.58	56	1.86	606	− 12.79	Yang et al. (2014)
Yichang	111.30	30.26	59	15.99	1186	− 7.39	Zhao et al. (2009)
Caotun	120.69	23.99	75	22.11	2027	− 6.42	Peng et al. (2010)
Dinghushan	112.55	23.16	90	21.87	1792	− 6.01	Liu et al. (2009a)
Taoyuan	111.50	28.92	106.5	17.25	1307	− 6.35	Yang et al. (2014)
Changshou	120.63	31.55	130	15.56	961	− 6.69	Yang et al. (2014)
Guilin	110.13	25.12	170	19.30	1852	− 6.2	Wu (2012)
Qianyanzhou	115.07	26.73	200	18.16	1514	− 4.4	Yang et al. (2014)
Taidong	121.09	22.84	250	23.21	2302	− 6	Peng et al. (2010)

Table 1 (continued)

Sites	Long (°E)	Lat (°N)	Alt (m)	Annual mean			Data sources
				T (°C)	P (mm)	$\delta^{18}O$ (‰)	
Huitong	109.72	26.87	300	16.73	1288	−4.79	Yang et al. (2014)
Naiman	120.70	42.92	358	7.14	439	−9.41	Yang et al. (2014)
Gaoling	109.10	34.55	378	13.17	658	−7.07	Yang et al. (2014)
Nanzheng	106.90	33	458	14.59	865	−7.14	Yang et al. (2014)
Hanzhong	107.00	33.1	512	14.76	841	−5.18	Wu (2012)
Bannan	101.53	21.9	560	20.16	1587	−6.67	Yang et al. (2014)
Puli	120.98	23.97	732	21.04	2474	−7.02	Peng et al. (2010)
Altai	88.14	47.86	737	3.63	187	−14	Yang et al. (2014)
Changbaishan	128.47	42.4	738	3.26	658	−9.98	Yang et al. (2014)
Majia	120.69	22.67	740	20.17	3579	−6.19	Peng et al. (2010)
Fukang	87.75	44.5	800	7.95	161	−12.31	Yang et al. (2014)
Yuanping	112.72	38.03	828.2	8.95	393	−7.62	Pang et al. (2015)
Changzhi	113.07	36.05	991.8	10.25	608	−10.55	Pang et al. (2015)
Yanan	109.47	36.6	1020	9.96	520	−7.17	Yang et al. (2014)
Baotou	109.85	40.67	1067	6.54	299	−7.87	Pang et al. (2015)
Datong	113.33	40.1	1067.2	7.26	370	−9.36	Pang et al. (2015)
Changwu	107.68	36.85	1200	9.83	594	−7.13	Yang et al. (2014)
Ansai	109.32	35.2	1200	9.33	484	−7.47	Yang et al. (2014)
Duolun	116.47	42.18	1245.4	2.85	389	−11.26	Pang et al. (2015)
Mengzi	103.23	23.23	1301.7	14.62	1354	−7.3	Li et al. (2016)
Simao	101.24	22.4	1302.9	19.01	1493	−7.57	Wu (2012)
Linze	100.12	39.35	1367	7.82	163	−8.2	Yang et al. (2014)
Minqin	103.05	38.38	1367.5	8.50	132	−11.67	This study
Jiuquan	98.47	39.77	1480	7.72	100	−11.3	Wu et al. (2011)
Wuwei	102.40	37.55	1531.5	−2.83	471	−6.16	This study
Tengchong	98.30	25.01	1648.7	14.49	1509	−8.03	Li et al. (2012b)
Gaolan	103.95	36.33	1668.5	8.65	297	−6.7	Chen et al. (2013)
Yinluoxia	100.20	38.81	1698	6.51	269	−6.5	Wu et al. (2011)
Wulin	121.31	24.35	1800	9.72	3194	−9.88	Peng et al. (2010)
Yuzhong	104.12	35.85	1874.4	6.79	373	−10.8	Chen et al. (2013)
Lishan	121.16	24.27	1980	10.55	3043	−8.32	Peng et al. (2010)
Huashan	110.08	34.48	2064.9	8.66	671	−10.13	Li et al. (2013a)
Xining	101.77	36.62	2261	6.06	386	−6.83	Yang et al. (2014)
Qilianxiang	102.37	37.33	2339	−4.15	491	−6.58	This study
Bilu	121.32	24.23	2350	8.33	3537	−10.44	Yao et al. (2013)
Alishan	120.81	23.51	2413	13.47	2627	−9.88	Peng et al. (2010)
Ailaoshan	101.02	24.53	2450	12.32	973	−9.2	Yang et al. (2014)
Xishui	100.29	38.57	2569	−2.04	397	−9.2	Wu et al. (2011)
Leibo	103.20	28.5	2600	5.72	942	−10.11	Han and Song (1998)
Jiangjiagou	103.50	23.1	2630	15.92	1459	−11.57	Guo et al. (2012)
Bomi	95.77	29.87	2737	2.79	741	−11.8	Yao et al. (2013)
Dayekou	100.30	38.5	2766	−5.03	428	−8.08	Wu (2012)
Wolong	102.97	30.85	2805	3.21	777	−12.01	Yang et al. (2014)
Geermu	94.89	36.42	2823	5.17	43	−6.7	Wu (2012)

Table 1 (continued)

| Sites	Long (°E)	Lat (°N)	Alt (m)	Annual mean			Data sources
				T (°C)	P (mm)	$\delta^{18}O$ (‰)	
Delingha	97.37	37.37	2981	3.86	173	− 7.74	Yang et al. (2014)
Gonggashan	101.75	30	3000	− 0.79	773	− 12.35	Song et al. (2015)
Huanglong	103.62	33	3247	− 0.27	754	− 15.3	Wang et al. (2012)
Lulang	94.73	29.77	3327	1.29	648	− 14.5	Yao et al. (2013)
Yangcun	91.88	29.88	3500	− 0.33	388	− 15.9	Yao et al. (2013)
Lhasa	91.13	29.7	3649	5.24	398	− 16.47	Yao et al. (2013)
Yushu	96.97	33.03	3682	− 0.38	542	− 13.14	Yao et al. (2013)
Nyalam	85.97	28.18	3810	0.37	493	− 12.4	Yao et al. (2013)
Jianjing	85.53	28.2	3880	− 0.55	504	− 14.33	Yao et al. (2013)
Qilain Site	96.50	39.5	4200	− 13.70	302	− 12.77	Yang et al. (2014)
Shiquanhe	80.08	32.5	4279	0.45	99	− 12.6	Yao et al. (2013)
Gaize	84.10	32.33	4416	0.19	81	− 9.95	Yao et al. (2013)
Baidi	90.43	29.12	4430	− 0.15	295	− 15.7	Yao et al. (2013)
Wenguo	90.35	28.9	4500	− 0.49	280	− 16.5	Yao et al. (2013)
Naqu	92.07	31.48	4507	− 0.76	431	− 16.6	Yao et al. (2013)
Tuotuohe	92.43	34.22	4533	− 3.77	280	− 11.9	Yao et al. (2013)
Nam Co	90.99	30.77	4730	− 1.54	416	− 18.4	Yang et al. (2014)
Dui	90.53	28.58	5030	− 2.97	287	− 18.6	Yao et al. (2013)
Anduo	91.68	32.29	5200	− 3.54	431	− 11.93	Yang et al. (2014)
Xixiabangma	102.97	30.85	2734	3.21	777	− 12.01	Yang et al. (2014)
Dunde	96.40	38.1	5325	− 14.05	297	− 9.93	Yao et al. (2013)
Geladandong	91.17	33.57	5720	− 13.46	398	− 12.34	Yao et al. (2013)
Malan	90.67	35.83	6056	− 13.42	270	− 12.58	Yao et al. (2013)
Puruoganggri	89.12	33.82	6200	− 14.22	302	− 14.67	Yao et al. (2013)
Guliya	81.48	35.28	6200	− 18.93	92	− 14.25	Yao et al. (2013)
East Rongbuk	86.97	28.02	6500	− 17.30	270	− 17.5	Yao et al. (2013)
Muztagata	75.10	38.28	7010	− 17.76	263	− 16.71	Yao et al. (2013)
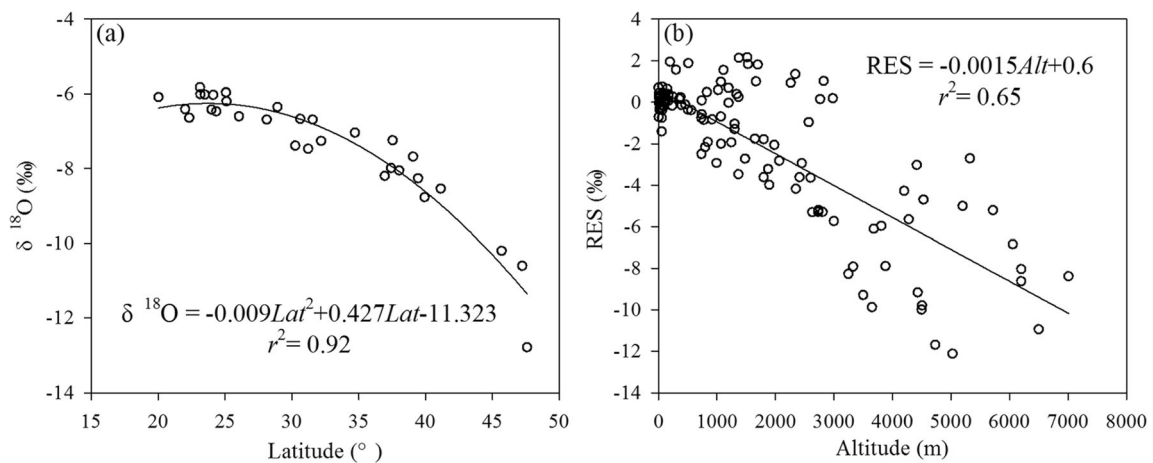
Fig. 2 **a** The fit of the $\delta^{18}O$ value and latitude of the sites ($n = 31$) that altitude below 200 m. **b** The fit of the residuals and elevations of all sites ($n = 117$); the residual is the difference between the measured $\delta^{18}O$ and the predicted $\delta^{18}O$ by Eq. (4)

In figure (a): $\delta^{18}O = -0.009Lat^2 + 0.427Lat - 11.323$, $r^2 = 0.92$

In figure (b): $RES = -0.0015Alt + 0.6$, $r^2 = 0.65$

7010 m. In order to quantitatively estimate the change of δ^{18}O value with altitude, first, the δ^{18}O values of all sites were predicted according to Eq. (4) and then the residuals of each station were calculated. Second, the residuals and elevations of each site were fitted by least squares regression:

$$\text{RES} = -0.0015\text{Alt} \ \left(r^2 = 0.65, P < 0.0001\right), \quad (5)$$

where RES is residual. The residual is the difference between the measured δ^{18}O and the modeled δ^{18}O by Eq. (4). RES = measured δ^{18}O-modeled δ^{18}O; modeled δ^{18}O was predicted by Eq. (4). As shown in Fig. 2b, the precipitation δ^{18}O value in China shows a linear decline with altitude, and the slope of Eq. (5) is − 0.0015. That is to say, the precipitation δ^{18}O value in China decreases with altitude by − 1.5‰ km^{-1}. This value is lower than that of the global average of − 2.8‰ km^{-1} (Poage and Chamberlain 2001) and − 2‰ km^{-1} (Bowen and Wilkinson 2002), but it is consistent with previous studies on China (Liu et al. 2009b; Yang et al. 2014).

The types of landforms in China are complex and diverse, and the variation of δ^{18}O value is influenced by many factors at the same time, such as topographic changes, local water vapor circulation, and sub-cloud secondary evaporation, which makes the decline rate of the δ^{18}O value in precipitation with altitude vary greatly in time and space. Therefore, the variation of the simulated precipitation δ^{18}O value with altitude in China actually simplifies the complexity of these influencing factors.

Based on BW model, the dependence of precipitation δ^{18}O value on latitude and altitude combination is described by adding the above Eqs. (4) and (5). Equation (6) provides a good estimate of the δ^{18}O value in precipitation ($r^2 = 0.64$, $P < 0.0001$, Fig. 3a) in the following:

$$\delta^{18}\text{O} = -0.009\text{Lat}^2 + 0.427\text{Lat}-0.0015\text{Alt}-11.323 \quad (6)$$
$$\left(r^2 = 0.64, P < 0.0001\right),$$

As shown in Fig. 3b, the range of residual varies from − 4.59 to 5.3‰. The mean bias error (MBE), mean absolute error (MAE), and root mean square error (RMSE) of the modeled values are − 0.5‰, 1.5‰, and 2.09‰, respectively.

3.2 Spatial distribution of model residual

The variation range of the residual between the measured δ^{18}O value and the modeled δ^{18}O value is − 4.6 to 5.2‰ (Fig. 3b). As shown in Fig. 4a, the distribution of residuals is mostly between − 1.5 and 1.5‰, which further indicates that the BW model can better estimate the spatial distribution of δ^{18}O value in precipitation over China. The spatial distribution of residual can reflect the influence of other important factors on the variation of precipitation isotope value in

different regions except latitude effect and altitude effect (Eq. 6), such as water vapor source and transport, local water vapor cycle, sub-cloud secondary evaporation, precipitation amount effect, and relative humidity (Dutton et al. 2005).

In order to reflect the influence of the above regional factors on the precipitation δ^{18}O value in different regions of China, we use the inverse distance weight (IDW) interpolation method to generate the spatial distribution map of the model 6 residuals (Fig. 4a). From Fig. 4a, we can see that the residuals are obviously larger in other regions except for the region of − 1.5 to 1.5‰, which indicates that the measured δ^{18}O values in these regions are significantly different from the simulated δ^{18}O values. Negative residual regions mainly occur in the southern Qinghai–Tibet Plateau, most of the Yunnan–Guizhou Plateau, and the Sichuan Basin; the south of the North Plain extends southward to the middle and lower reaches of the Yangtze river basin, the north of Taiwan, the southern slope of the Altai Mountains, and the Sanjiang Plain in Northeast China. These areas may also be affected by precipitation amount effect or Indian Ocean water vapor transport (Zhang and Yao 1998; Yao et al. 2013), making the measured of precipitation δ^{18}O value lower than the estimated δ^{18}O value. On the contrary, in the western and central regions of northwest arid region, such as the Taklimakan Desert in the Tarim Basin, Badain Jilin Desert in Inner Mongolia, and the north and west of Qinghai–Tibet Plateau, these areas may be affected by local continental water vapor and secondary evaporation (Tian et al. 2007; Liu et al. 2008), making the simulated δ^{18}O value lower than the measured δ^{18}O value.

3.3 Spatial distribution of δ¹⁸O value in precipitation over China

In order to reflect the combined effects of various factors on the precipitation δ^{18}O value, the residual grid (Fig. 4a) was added to the grid generated by Eq. (6) to produce the spatial distribution map of precipitation δ^{18}O value over China (Fig. 4b). Figure 4b represents our best estimation of precipitation δ^{18}O value and can roughly show the spatial distribution of precipitation δ^{18}O value over China.

It can be seen from the Fig. 4b that the high value region of δ^{18}O is mainly distributed in the eastern monsoon region and the northwest arid region, and the low value area is distributed in the southwest of Qinghai–Tibet Plateau region and the northeastern region of China. In the eastern monsoon region, including most of the North China Plain, the Han River basin, the Sichuan basin, the Yunnan–Guizhou Plateau, the Yarlung Zangbo River basin, and the plains areas of Taiwan Island, the δ^{18}O value is highest, which ranged from − 8 to −6.3‰. In the western part of the Qinghai–Tibet Plateau and the northwest–southeast direction curved mountain, Altai Mountain, Tianshan, and other mountains, the δ^{18}O value is lowest, which is between − 18.8 and − 16‰. Comparing our research

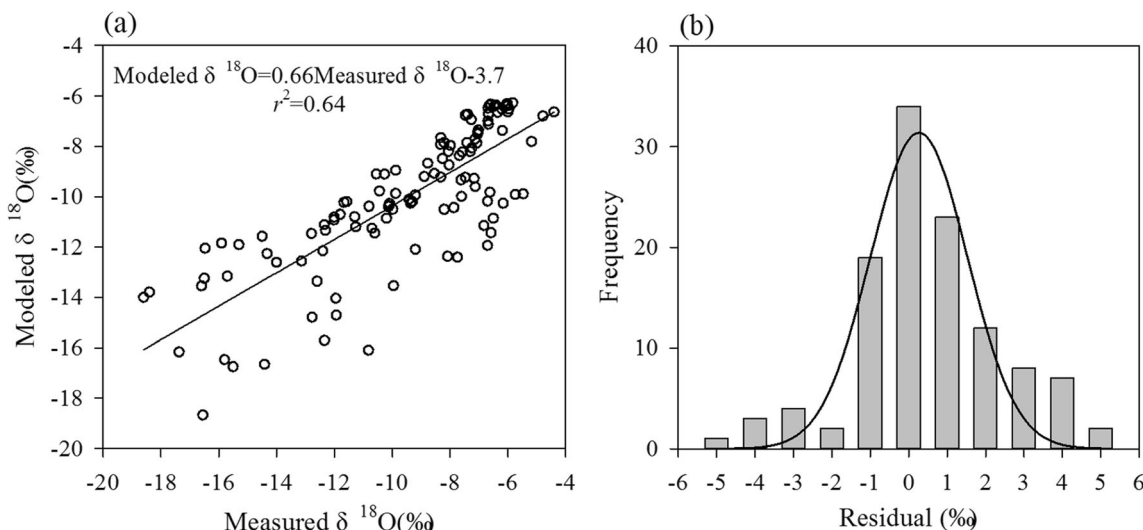**Fig. 3** **a** Measured $\delta^{18}O$ value versus $\delta^{18}O$ value modeled by Eq. (6) of 117 sites. **b** The frequency distribution of residual between measured $\delta^{18}O$ value and modeled $\delta^{18}O$ value

results with other studies (Liu et al. 2009b; Yang et al. 2014), it is found that the range of the maximum $\delta^{18}O$ value becomes smaller, and the range of the minimum $\delta^{18}O$ value becomes larger, that is, the range of variation of $\delta^{18}O$ becomes smaller, but the $\delta^{18}O$ value is higher in most areas, especially in the central basin and the eastern low latitude plain. Obviously, the high value areas of $\delta^{18}O$ are mainly distributed in basins, valleys, and low-altitude plains. The low-value areas are mainly distributed in high-latitudes and high-altitude areas and are strongly influenced by latitude effect and elevation effect.

In the eastern monsoon region, the $\delta^{18}O$ value tends to decrease with the increase of latitude; when in the northeast

region, the $\delta^{18}O$ value is the lowest. Although the isotope values of precipitation in the monsoon region are generally higher, but the latitude effect can still be exhibited. The Qinghai–Tibet Plateau is affected by high altitude and special topography. Except for the plateau marginal zone, the Qaidam Basin, and the eastern low-altitude zone, the $\delta^{18}O$ value of the plateau is low, and its spatial distribution is greatly affected by the northwest–southeast arc mountain. In the Northwest arid regions China, except for the low $\delta^{18}O$ value in the mountainous area, the high value area of $\delta^{18}O$ extends from the Tarim Basin to the Hexi area of Gansu and the Middle East area of Inner Mongolia, mainly affected by local water vapor cycle and local evaporation under arid environment.
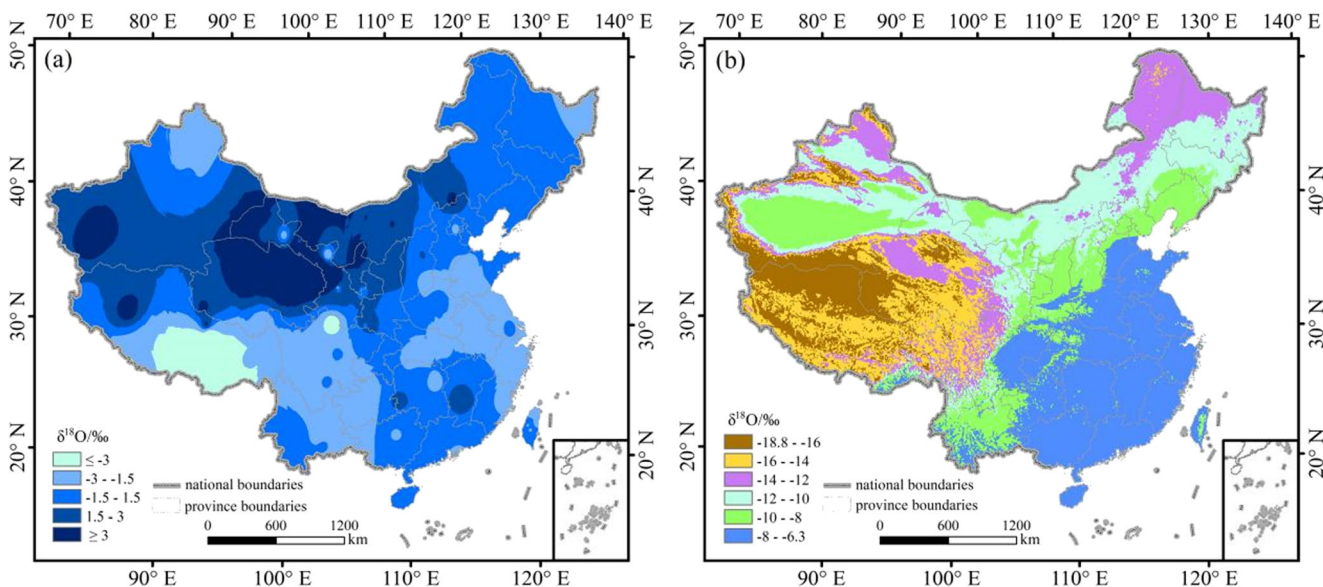

Fig. 4 **a** Spatial distribution of residuals using inverse-distance-weighted method over China. **b** Spatial distribution of $\delta^{18}O$ value in precipitation over China based on a sum of residual distribution map (**a**) and $\delta^{18}O$ value estimated by Eq. (6)

3.4 Temperature and precipitation amount dependence of δ¹⁸O in precipitation

China's temperature and precipitation vary greatly from north to south and from east to west. Therefore, China is divided into several sub-regions according to the relative uniformity of the underlying surface and climatic conditions (Fig. 1). Figure 5 shows the regression of δ¹⁸O values and temperature and precipitation amount for each sub-region. In the southeast monsoon region, although it can be affected by the southeast monsoon water vapor, there are great differences between the southern region and northern region. In the southern region, as the temperature rises and the precipitation increases, the δ¹⁸O value is positively correlated with the temperature and negatively correlated with the precipitation amount (Fig. 5a, b), that is, there are both temperature effect and precipitation amount effect. However, the temperature effect in the southern region is more significant than the precipitation amount effect and is closest to the subtropical ocean water vapor source. The δ¹⁸O value in the precipitation water vapor is high (Pang et al.
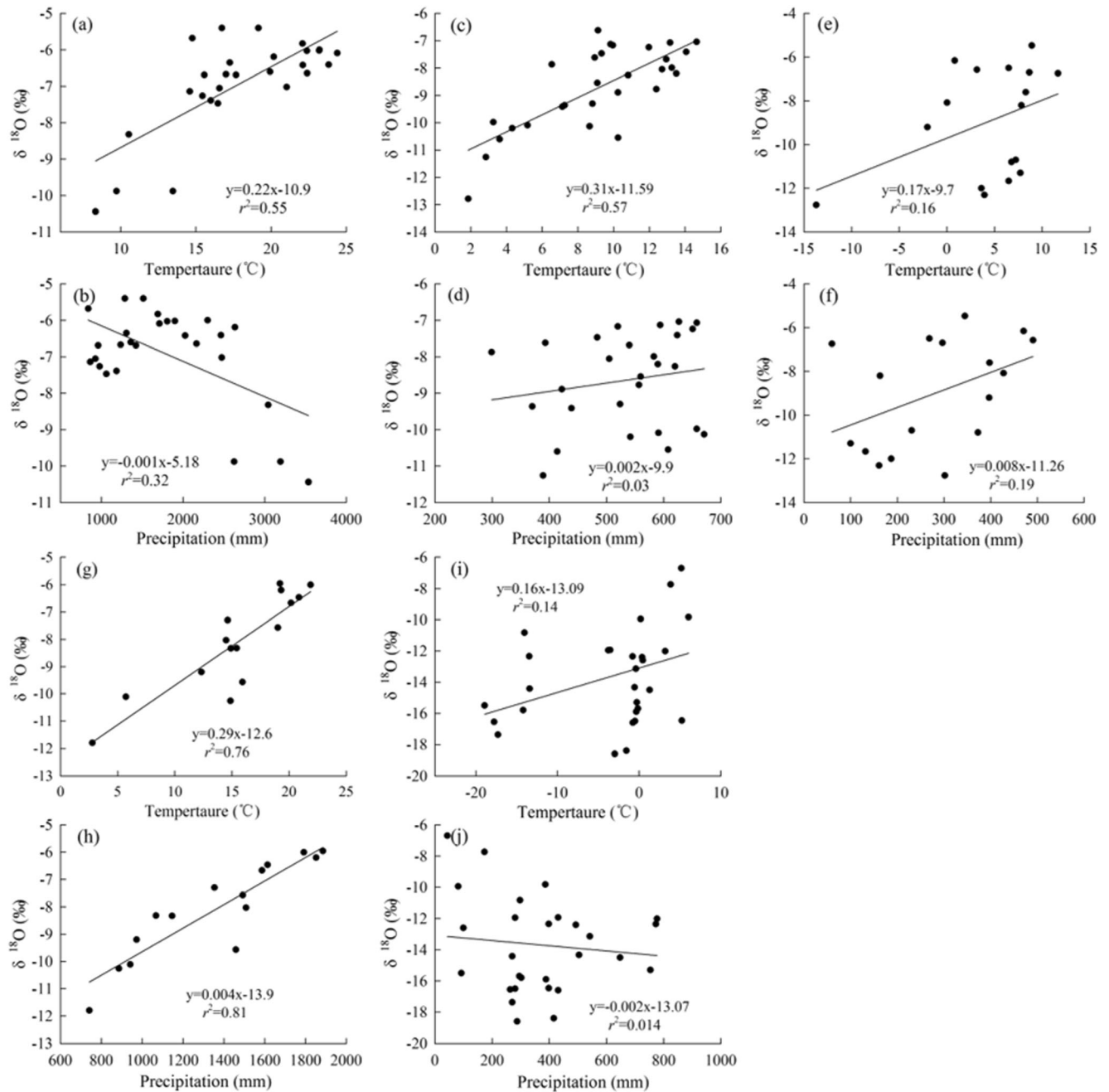
Fig. 5 The variation of δ¹⁸O values in the southern region (**a, b**) and northern region (**c, d**), northwest arid region (**e, f**), southwest monsoon region (**g, h**), and Qinghai–Tibet Plateau (**i, j**) with temperature and precipitation in China

2005), and the high-value region of precipitation $\delta^{18}O$ value is formed in the southern region with good hydrothermal combination (Fig. 4b). In the northern region, the $\delta^{18}O$ value is positively correlated with temperature and precipitation (Fig. 5c, d), that is, there is a temperature effect but no precipitation amount effect, indicating that the precipitation amount effect is more obvious in low latitude area and the temperature effect is more obvious in middle- and high-latitude areas, which are more consistent with the previous scholars' conclusions (Zhang and Yao 1998; Yamanaka et al. 2007).

In the northwest arid area, the temperature effect is considered to be the decisive factor in many factors affecting the precipitation isotope composition, and the $\delta^{18}O$ value in precipitation water vapor is originally high due to the influence of local continental water vapor cycle and secondary evaporation. As shown in Fig. 5e, f, there is indeed a temperature effect and no precipitation effect in the northwest arid area, but the correlation of the $\delta^{18}O$ value with temperature and precipitation is weaker than that in other regions. This may be due to the sparse and uneven distribution of sites in the northwest arid region (Fig. 1), which makes the existing sites unable to represent the overall situation of the region. There is a positive correlation between the $\delta^{18}O$ value and temperature and precipitation in the southwest monsoon region, and the correlation is high (Fig. 5g, h). In the Qinghai–Tibet Plateau region, there are still temperature effect and precipitation effect, but the correlation between $\delta^{18}O$ value and temperature and precipitation is also weak (Fig. 5i, j), which is related to the special role of high terrain.

3.5 Water source signatures reflected by $\delta^{18}O$ in precipitation

Figure 6a shows the annual average vapor flux, from which we can see the water vapor source and transport of China. Figure 6b shows the water vapor flux divergence, which represents the net income and expenditure of water vapor. In the eastern monsoon region, the westerly water vapor transport, the southwest monsoon, and southeast monsoon water vapor transport are converged in the south of the Yangtze River and the conveying intensity can reach 1200–1500 kg m^{-1} s^{-1}. In the south and east of the convergence area, the water vapor mainly comes from the southwestern monsoon of the Indian Ocean and the southeastern monsoon of the Pacific Ocean. In the west and north of the convergence area, the water vapor is mainly transported by the westerly. Water vapor diffuses northward and eastward from the convergence area, forming a positive diffusion area in southeastern China, and the northward water vapor transport is weakened until the northernmost Mohe is only 300 kg m^{-1} s^{-1}. The corresponding $\delta^{18}O$ value in Fig. 4b also shows a decreasing trend with the increase of latitude.

The Indian Ocean water vapor is the main source of precipitation in the southern of the Qinghai–Tibet Plateau (Tian et al. 2001). In the west of China, the southwest monsoon water vapor transport from south to north is weakening, and the proportion of westerly water vapor and local continental air mass is gradually increasing (Fig. 6a). According to Tian et al. (2001), Tanggula Mountain is an important boundary. As shown in Fig. 4b, the precipitation $\delta^{18}O$ value in western China decreases first and then increases from south to north. Figure 6b shows that in the south of the Loess Plateau and the north of Sichuan basin is the water vapor flux negative divergence area, i.e., the net income area of water vapor. In the south and southeast of the Qinghai–Tibet Plateau, due to the influence of high topography, water vapor around the flow and overturned transport to form the northwest–southeast water vapor convergence zone, which is one of the sources of precipitation water vapor in these areas, and the corresponding $\delta^{18}O$ value is also larger. Therefore, the spatial distribution of precipitation $\delta^{18}O$ values can well track water vapor and its transport trajectories from different sources.
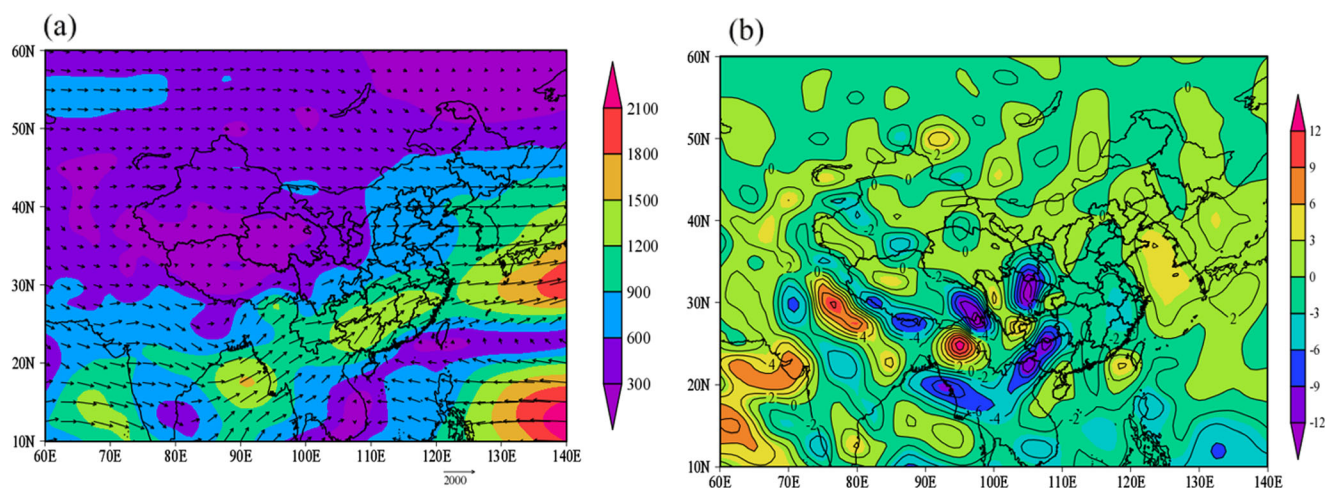
4 Conclusion

A model was built to simulate the $\delta^{18}O$ value in precipitation by stepwise regression of $\delta^{18}O$ value and latitude and altitude of 117 sites in China. The spatial distribution map of precipitation $\delta^{18}O$ value in China with high precision was generated by spatial interpolation, and the variation of $\delta^{18}O$ value in different climatic regions and its influencing factors was analyzed. The simulation results show that the BW model can better simulate precipitation $\delta^{18}O$ value in China. The main area of the model residual distribution in China is between -1.5 and 1.5‰. Other residual deviation regions can be used to explain that the precipitation $\delta^{18}O$ values are affected by other local factors besides latitude effect and altitude effect, while the spatial distribution of $\delta^{18}O$ values over China can simultaneously reflect latitude effect, altitude effect, and regions other influence factors. The $\delta^{18}O$ value is restricted by topography; the high value areas are mainly distributed in basins, valleys, and plains at low altitude; and the low value areas are mainly distributed in high latitude and high altitude areas and some mountain areas, which are affected by elevation effect. In the southeast monsoon region, the latitude effect of isotope value variation is reflected from south to north, but the difference between the south and north indicates that the precipitation amount effect is obvious in the low latitude areas and the temperature effect is obvious in the middle and high latitude areas. In the same latitude area, the inland basins in the northwest arid region have formed high isotope value areas, which indicate that the inland water vapor cycle and secondary evaporation have strong influence on the area. In the Qinghai–Tibet Plateau, the isotope values are generally low due to the influence of high topography (altitude effect), the southwest monsoon weakens from south to north, and the westerly and inland water vapor cycles strengthen. The corresponding isotope values decrease from south to north and then increase. The spatial distribution of precipitation $\delta^{18}O$ values can track water vapor from different sources in China.

References

Bowen GJ, Revenaugh J (2003) Interpolating the isotopic composition of modern meteoric precipitation. Water Resour Res 39(10). https://doi.org/10.1029/2003WR002086

Bowen GJ, Wilkinson B (2002) Spatial distribution of $\delta^{18}O$ in meteoric precipitation. Geology 30(4):315–318

Chen F, Zhang M, Ma Q et al (2013) Characteristics of $\delta^{18}O$ in precipitation and water vapor sources in Lanzhou City and its surrounding area. Environ Sci 34(10):3755–3763

Clark I, Fritz P (1997) Environmental isotopes in hydrology. Lewis Publishers, New York, p 328

Craig H (1961) Isotopic variations in meteoric waters. Science 133(3465):1702–1703

Daley TJ, Mauquoy D, Chambers FM (2012) Investigating late Holocene variations in hydroclimate and the stable isotope composition of precipitation using southern South American peatlands: a hypothesis. Clim Past Discuss 8(1):595–620

Dansgaard W (1953) The abundance of ^{18}O in atmospheric water and water vapour. Tellus 5(4):461–469

Dutton A, Wilkinson BH, Welker JM, Bowen GJ, Lohmann KC (2005) Spatial distribution and seasonal variation in $^{18}O/^{16}O$ of modern precipitation and river water across the conterminous USA. Hydrol Process 19(20):4121–4146

Edwards TWD, Birks SJS, Amour NA et al (2010) Progress in isotope tracer hydrology in Canada. Hydrol Process 19(1):303–327

Fernandoy F, Meyer H, Tonelli M (2011) Potential of the stable water isotope composition of precipitation and firn cores as a proxy for climate reconstruction at the Northern Antarctic Peninsula region. Neuroreport 15(8):1315–1319

Fick SE, Hijmans RJ (2017) WorldClim 2: new 1-km spatial resolution climate surfaces for global land areas. Int J Climatol 37(12):4302–4315. https://doi.org/10.1002/joc.5086

Gat JR (1980) The isotopes of hydrogen and oxygen in precipitation. In: Fritz P, Fontes JC (eds) Handbook of environmental isotope geochemistry. Elsevier, Amsterdam, pp 21–47

Gat JR (1996) Oxyge and hydrogen isotopes in the hydroligic cycle. Annu Rev Earth Planet Sci 24:225–262

Good SP, Noone D, Kurita N, Benetti M, Bowen GJ (2015) D/H isotope ratios in the global hydrologic cycle. Geophys Res Lett 42(12):5042–5050

Guo X, Su F, Hong Y et al (2012) Characteristics of hydrogen and oxygen isotopes in rainy season precipitation in Jiangjiagou watershed. Research of Soil and Water Conservation 19(2):82–76 (in Chinese)

Han Q, Song S (1998) Study on D, ^{18}O isotopes of precipitation in Leibo area, Southwest Sichuan. Geological Science and Technology Information s2:106–110 (in Chinese)

He YQ, Yao TD, Yang MX, Shen YP (2000) Contemporary significance of snow and ice indicated by the record in a shallow ice core from a temperate glacier in southwestern monsoon region. J Glaciol Geocryol

Hoffmann G, Heimann M (1997) Water isotope modeling in the Asian monsoon region. Quat Int 37(2):115–128

Huang J, Tan H, Wang R, Wen X et al (2015) Hydrogen and oxygen isotopic analysis of perennial meteoric water in Northwest China. J China Hydrol 35(1):33–39

Johnson KR, Ingram BL (2004) Spatial and temporal variability in the stable isotope systematics of modern precipitation in China: implications for paleoclimate reconstructions. Earth Planet Sci Lett 220(3–4):365–377

Li X, Zhang M, Wang S et al (2013a) Spatial and temporal variations of hydrogen and oxygen isotopes in precipitation in the Yellow River Basin and its environmental significance. Acta Geol Sin 87(2):269–277

Li G, Zhang X, Zhang X et al (2013b) Stable hydrogen and oxygen isotopes characteristics of atmospheric precipitation from Tengchong, Yunnan. Resources and Environment in the Yangtze Basin 22(11):1458–1465 (in Chinese)

Li J, Pang Z, Kong Y et al (2014) Contrasting seasonal distribution of stable isotopes and deuterium excess in precipitation over China. Fresenius Environ Bull 23(9):2074–2085

Li G, Zhang X, Xu Y et al (2016) Characteristics of stable isotopes in precipitation and their moisture sources in Mengzi region, Southern Yunnan. Environ Sci 37(4):1313–1320

Liu J, Song X, Yuan G et al (2008) Characteristics of δ^{18}O in precipitation over Northwest China and its water vapor sources. Acta Geograph Sin 63(1):12–22

Liu J, Song X, Yuan G a (2009a) Characteristics of δ^{18}O in precipitation over eastern monsoon China and the water vapor sources. Chin Sci Bull. https://doi.org/10.1007/s11434-009-0202-7

Liu Z, Tian L, Yao T et al (2009b) Spatial distribution of δ^{18}O in precipitation over China. Chin Sci Bull 54(6):804–811

Pang H, He Y, Zhang Z et al (2005) Sources of in δ^{18}O monsoon precipitationand monsoon vapor. Chin Sci Bull 50(20):2263–2266

Pang S, Zha OS, Wen R et al (2015) Spatial and temporal variation of stable isotopes in precipitation in the Haihe River basin. Chin Sci Bull 60:1218–1226. https://doi.org/10.1360/N972014-01040

Peng T, Wang C, Huang C et al (2010) Stable isotopic characteristic of Taiwan's precipitation: a case study of western Pacific monsoon region. Earth Planet Sci Lett 289(3–4):357–366

Poage MA, Chamberlain CP (2001) Empirical relationships between elevation and the stable isotope composition of precipitation and surface waters: considerations for studies of paleoelevation change. Am J Sci 301(1):1–15

Pu T, He Y, Zhu G, Zhang N, Du J, Wang C (2013) Characteristics of water stable isotopes and hydrograph separation in baishui catchment during the wet season in mt.yulong region, south western China. Hydrol Process 27(25):3641–3648

Samuels-Crow KE, Galewsky J, Sharp ZD et al (2014) Deuterium excess in subtropical free troposphere water vapor: continuous measurements from the Chajnantor plateau, Northern Chile. Geophys Res Lett 41(23):8652–8659

Sengupta S, Sarkar A (2006) Stable isotope evidence of dual (Arabian sea and Bay of Bengal) vapour sources in monsoonal precipitation over North India. Earth Planet Sci Lett 250(3–4):511–521

Sjolte J, Hoffmann G, Johnsen SJ et al (2011) Modeling the water isotopes in Greenland precipitation 1959–2001 with the meso-scale model remo-iso. J Geophys Res-Atmos 116(D18):1110–1117

Song X, Liu J, Sun X, Yuan G, Xin L, Shi-Qin W et al (2007) Establishment of Chinese network of isotopes in precipitation (CHNIP) based on CERN. Adv Earth Science 22(7):738–747

Song C, Sun X, Wang G (2015) A study on precipitation stable isotopes characteristics and vapor sources of the subalpine Gongga mountain, China. Resources and Environment in the Yangtze Basin 24(11): 1860–1869 (in Chinese)

Tian L, Yao T, Sun W et al (2001) Relationship between δD and δ^{18}O in precipitation on north and south of the Tibet Plateau and moisture recycling. Sci China Ser D 31(3):214–220

Tian L, Yao T, Macclune K et al (2007) Stable isotopic variations in West China: a consideration of moisture sources. J Geophys Res-Atmos 112(D10):185–194

Tindall JC, Valde SPJ, Sime LC (2009) Stable water isotopes in HadCM3: isotopic signature of El Niño–Southern Oscillation and the tropical amount effect. J Geophys Res-Atmos 114(D4):83–84

Wang H, Zhang J, Liu Z (2012) Indications of the hydrogen and oxygen isotopes in precipitation for climate change in Huanglong, Sichuan. Carsologica Sinica 31(3):253–258 (in Chinese)

Wang S, Zhang M, Bowen GJ, Liu X, Du M, Chen F et al (2018) Water source signatures in the spatial and seasonal isotope variation of Chinese tap waters. Water Resour Res 54(11):9131–9143

Wu H (2012) Study on the characteristics of stable isotopes different bodies in the mid-and-lower reaches of Xiangjiang River. Hunan Norm Univ, ChangSha, p 18–20

Wu J, Yang Q, Ding Y et al (2011) Variations and simulation of stable isotopes in precipitation in the Heihe River Basin. Environ Sci 32(7):1857–1866

Yamanaka T, Tsujimura M, Oyunbaatar D, Davaa G (2007) Isotopic variation of precipitation over eastern Mongolia and its implication for the atmospheric water cycle. J Hydrol 333(1):21–34

Yang J, Qin X, Wu J et al (2014) The application of modified BW method in studying spatial distribution of δ^{18}O in precipitation over China. J Glaciol Geocryol 36(6):1430–1439

Yao T, Masson-Delmotte V, Gao J, Yu W, Yang X, Risi C, Sturm C, Werner M, Zhao H, He Y, Ren W, Tian L, Shi C, Hou S (2013) A review of climatic controls on δ^{18}O in precipitation over the Tibetan Plateau: observations and simulations. Rev Geophys 51(4):525–548

Zhang X, Yao T (1998) Distributional features of δ^{18}O in precipitation in China. Acta Geograph Sin 1998(4):356–364

Zhang X, Sun Z, Guan H, Zhang X, Wu H, Huang Y (2012) GCM simulations of stable isotopes in the water cycle in comparison with GNIP observations over East Asia. Acta Meteor Sin 26(4):420–437

Zhao J, Wei B, Xiao S et al (2009) Stable isotopic characteristics of atmospheric precipitation from Yichang, Hubei. Trop Geogr 29(6): 526–531

Zhao LJ, Yin L, Xiao HL, Cheng GD, Zhou MX, Yang YG, Li CZ, Zhou J (2011) Isotopic evidence for the moisture origin and composition of surface runoff in the headwaters of the Heihe river basin. Sci Bull 56(z1):406–415

Zhu G, Li J, Shi P, He YQ, Cai A, Tong HL, Liu YF, Yang L (2016) Relationship between sub-cloud secondary evaporation and stable isotope in precipitation in different regions of China. Environ Earth Sci 75(10):876

Zhu G, Guo H, Qin D, Pan H, Zhang Y, Jia W, Ma X (2019) Contribution of recycled moisture to precipitation in the monsoon marginal zone: estimate based on stable isotope data. J Hydrol 569:423–435